Iris Recognition based on Wavelets

S V Sheela
B M S College of Engineering
Bangalore, India.

P A Vijaya
Malnad College of Engineering
Hassan, India

ABSTRACT
Recognition refers to the problem of establishing a subject's identity from a set of already known identities. Iris recognition system identifies a person from the database of iris images. Iris patterns form distinguishing characteristics for an individual. The potency of iris recognition lies in its textual information. Iris based security systems capture iris patterns of individuals and match the patterns against the record in available databases. In this paper, wavelet decomposition is applied on iris patterns. The magnitude of coefficients aid in the generation of unique code for recognition. The recognition rate of 100% is achieved.

Keywords
Wavelet decomposition, unique code, magnitude of detailed coefficients, core and non-core segments

1. INTRODUCTION
Biometric is a metric of apparent nontransferable uniqueness provided by user's presence. Biometrics are extremely convenient form of providing identity and cannot

be lent to another individual. The digital impersonation provides usage of biometrics in security techniques. A measurable physical characteristic is more reliable to eliminate identity theft. Iris biometry is used to recognize an individual in a natural and intuitive way. Iris is the annular ring between pupil and sclera of eye. The sclera is the white region of connective tissues surrounding iris. The pupil is the darkest region in eye. The iris is highly protected and non-invasive. The structure of iris exhibits long-term stability. The texture of the iris presents distinguishing characteristics. The variations in the gray level intensity values distinguish two individuals. The attributes important for large-scale identity programs are accuracy, algorithm speed and template size. The security systems, database authentication systems and secure transactions are major applications. The iris recognition algorithms need to be developed and tested in diverse environment and configurations. Research issues are based on iris localization, normalization, occlusion, segmentation,

liveness detection and handling noisy and degraded iris images. The occlusion is due to eyelid and eyelashes. Iris liveness detection differentiates live subject from a photograph, a video playback, a glass eye or other artifacts. Biometric security techniques look for unique physiological characteristics that remain constant and difficult to fake. A blend of acquisition, feature extraction and classification has evidently become technology oriented in e-commerce and m-commerce applications. The most common features are x-y coordinates of pupil, intensity value, radius of pupil, radius of iris, eye corners and ratio of limbus diameter to pupil diameter. The derived features are intensity gradient, phase information, texture difference, zero crossings, moment values, wavelet decomposition coefficients, local intensity variations, independent component analysis, hierarchical texture information, fractal dimension, zerotree wavelet code, local-global graphs and mean/standard deviation of image. The general classifiers used are support vector machine, radial basis function, genetic algorithm, component analysis, *k*-means, fuzzy *k*-means, *k*-nearest neighbor and neural networks. The metrics used to identify an individual are sequence codes such as iriscode.

2. PROLOGUE
2.1 Connected Components Labeling
The Connectivity between pixels of gray scale images is determined based on gray level intensity values and spatial adjacency [1]. The neighborhood system NS_d is defined for d=4, 8. Two pixels p_1, $p_2 \in NS_4$ are called 4-adjacent, if they are vertical or horizontal neighbors. The pixels p_1, $p_2 \in NS_8$ are called 8-adjacent, if they are vertical, horizontal or diagonal neighbors. A set of pixels C is d-connected if for every pair of pixels c_i, $c_j \in C$, there exists a sequence of pixels $c_i,\ldots,c_j$ such that (i) all pixels in the sequence share same intensity value and (ii) each consecutive pair in the sequence is d-adjacent [3]. The region of connected pixels is called connected component [4]. The distinct regions in an image are identified.

Connected component labeling assigns a label to each pixel representing the region to which it belongs. The labeling process scans the image in horizontal and vertical directions for white pixels. Each unlabeled pixel $I(x, y)$ is considered. The 8-connected neighbors, (m, n) are listed. The criteria is based on the presence of same intensity value in the neighboring pixels. A label is assigned in label matrix, M_{label} corresponding to position (x, y), if $I(m, n)$ is equal to $I(x, y)$. The method labels all pixels in the 8-connected region to which pixel belongs [4]. The sequence of steps involved in labeling process is shown in Figures 1(a)-(e). The connected components are labeled using (1).

$$[M_{label}, n] = com_{label}(B) \tag{1}$$

where n is the number of connected components and B is the binary image.

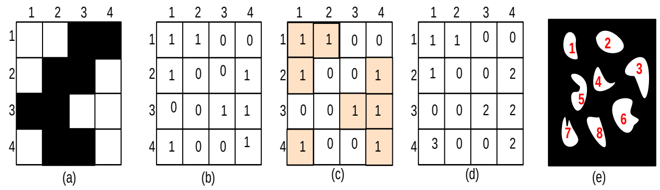

Fig 1. (a) Binary image (b) Intensity values (c) Connected components (d) Label matrix (e) An instance of component labelling

The area of all white pixels is summation of individual pixel areas in the image. In a 2x2 neighborhood, considering only the white pixels, the area of one pixel is 0.25, two adjacent pixels is 0.5, two diagonal pixels is 0.75, three pixels is 0.875 and four pixels is 1. The area is determined using (2) for each connected component.

$$C(k) = com_{area}(k)\text{, } k=1,2,\ldots n \text{ and } M_{label} = k \qquad (2)$$

$$m_{com} = \max(C) \qquad (3)$$

The vector C consists of component areas. The component with maximum area is determined using (3).

2.2 Discrete Wavelet Transform

Wavelet transform provides the time-frequency representation. In case of discrete wavelet transform (DWT), filters of different cutoff frequencies are used to analyze the signal at different scales [5]. Wavelets are mathematical functions that divides the data into different frequency components to analyze each component with a resolution matched to its scale [6]. Wavelet decomposition involves a pair of waveforms, the wavelet function and the scaling function. The wavelet function represents high frequencies corresponding to the detailed parts of an image. The scaling function represents the low frequencies or smooth parts of an image. The DWT analyzes the signal by decomposing the signal into a coarse approximation and detail information. The scaled and translated basis functions in 2D DWT is given by (4) and (5).

$$\phi_{k,p,q}(x,y) = 2^{k/2}\varphi(2^k x - p, 2^k y - q) \qquad (4)$$

$$\psi^i_{k,p,q}(x,y) = 2^{k/2}\psi^i(2^k x - p, 2^k y - q) \qquad (5)$$

where i is the index to identify the directional wavelets in terms of horizontal, vertical and diagonal components.

In two level decomposition, the upper left quadrant is the approximation of the source image. The upper right, lower left and lower right represent vertical, horizontal and diagonal details of the source. The approximation at level 1 is decomposed into four components at level 2. The wavelet transform outputs at each level the approximation, horizontal detail, vertical detail and diagonal detail. The size of each subimage is reduced to quarter of the source image.

The Haar basis is obtained with a multiresolution of piecewise constant functions. The scaling function is $\phi = 1_{[0,1]}$. The wavelet function is given by $\psi(t) = -1$ if $0 \le t \le 0.5$, 1 if $0.5 \le t \le 1$, 0 otherwise. It is the only symmetric wavelet with the advantages of being fast and memory efficient. Haar wavelets is conceptually simple, but not suitable for approximating smoothing functions that is required in applications like compression. Haar wavelet has only one vanishing moment. The vanishing moment of v indicates that any polynomial signal up to order $v-1$ is represented completely in scaling space.

Daubechies family of scale functions have finite vanishing moments. This property is useful for local analysis and insures the number of non-zero coefficients in the associated filter to be finite [7]. The scaling function is given by $\phi(x) = \sum_{i=0}^{N-1} p_i \phi(2x - i)$ and wavelet function is $\psi(x) = \sum_{i=2-N}^{1} (-1)^i p_{1-i}\phi(2x-i)$ where $i=1,2,\ldots, N-1$ are the filter coefficients [8]. Daubechies wavelets are asymmetric. By optimizing the real coefficients $R(e^{iw})$ of the minimum degree polynomial $P((2 - e^{iw} - e^{-iw})/4)$, the linear phase and symmetric property is obtained. Thesymmetric wavelets are the symlets. Coiflet family of wavelets have v vanishing moments. The scaling functions are based on the constraints, $\int \phi(t)dt = 1$ and $\int p^k \phi(p)dp = 0$ for $1 \le k \le v$. The coiflets are useful for establishing precise quadrature formulas. Biorthogonal wavelets are families of compactly supported symmetric wavelets. The symmetry of the filter coefficients provides linear phase of the transfer function [7]. Two scaling functions, $\phi, \tilde{\phi}$ and two wavelet functions, $\psi, \tilde{\psi}$ are defined such that $\int \psi_{j,k}(x)\tilde{\psi}_{j',k'}(x)dx = 0$ for $j \ne j'$ or $k \ne k'$ and $\int \phi_{0,k}(x)\tilde{\phi}_{0,k'}(x)dx = 0$ for $k \ne k'$. The properties of analysis are concentrated on $\tilde{\psi}$ function and synthesis on ψ function.

3. RELATED WORK

The iris recognition system by J.Daugman use phase-based approach 10. The representation of iris texture is binary coded by quantizing the phase response of a texture filter using quadrature 2D Gabor wavelets into four levels. Iris codes are generated and Hamming Distance is used as a measure of dissimilarity. Continuing the Daugman's method, Karen Hollingsworth has developed techniques for improving recognition rates [10]. The techniques include fragile bit masking, signal level fusion of iris images, detecting local distortions in iris texture and analyzing the effects of pupil dilation. The experiments are conducted on ICE database. The system developed by Wildes is based on texture analysis [11]. The Laplacian of Gaussian (LoG) is applied to the image at multiple scales and the resulting Laplacian pyramid constructed with different levels serve as basis for further processing. Iris recognition system developed by Li Ma is characterized by local intensity variations [12]. The sharp variation points of iris patterns are recorded as features. The feature extraction generates 1D intensity signals considering the information density in the angular direction. The feature values are the mean and the average absolute deviation of the magnitude of each 8x8 block in the filtered image. The method by Li Ma was further improved by Zhenan Sun where in the local feature based classifier was combined with an iris blob matcher [13]. The blob matching aimed at finding the spatial correspondences between the blocks in the input image and that in the stored model. The similarity is based on the number of matched block pairs. The block attributes are recorded as centroid coordinates, area and second order central moments. H. Proenca proposed a moment-based texture segmentation algorithm, using second order geometric moments of the image as texture features [14]. The iris recognition system by Aditya Abhyankar is based on biorthogonal 5/3 tap wavelets [15]. The experiment is conducted on CASIAv1 database. The match-score calculation was performed using Hamming Distance and FRR of 4.2% is obtained with a threshold of 0.25. The method by Agus Harjoko use 1D coiflet wavelet for iris recognition [16]. Coiflet wavelet transform is applied to the iris image from CASIAv1 database. The second order wavelets was implemented with four decomposition levels.

Hamming Distance is used as decision criteria and a success rate of 84.25% was obtained.

4. PROPOSED METHOD

4.1 Preprocessing

The 640x480 sized eye image *I* is shown in Figure 2(a). The histogram *H,* of *I* provides the count of pixels *pc* for each intensity value using (6). The first peak in the histogram is the threshold value *h* computed using (7). The intensity values less than or equal to *h* are obtained as a intermediate binary image *B* using (8). The white pixels in *B* corresponds to pupil and eyelashes as shown in Figure 2(b). The intensity values greater than h is the sclera and eyelids.

$$pc = H(I(x, y)) \tag{6}$$

$$h = \max(pc) \tag{7}$$

$$B = I(x, y) <= h \tag{8}$$

The result of determining maximum area of connected components is a binary image such that pupil area is white and other parts of image are black as shown in Figure 2(c). The maximum and minimum values of x-coordinates corresponding to the white pixels, x_{max} ,x_{min} are identified. Similarly, the maximum and minimum values of y-coordinates corresponding to white pixels, y_{max}, y_{min} are determined. The centre of pupil is calculated using $x_c = (x_{max} + x_{min})/2$ and $y_c = (y_{max} + y_{min})/2$. The radius of both axes is determined using $rad_1 = (x_{max} - x_{min})/2$ and $rad_2 = (y_{max} - y_{min})/2$. The pupil radius, $rad_p = max(rad_1, rad_2)$. A mapping is achieved to original gray scale image using coordinates of pupil center and radius.

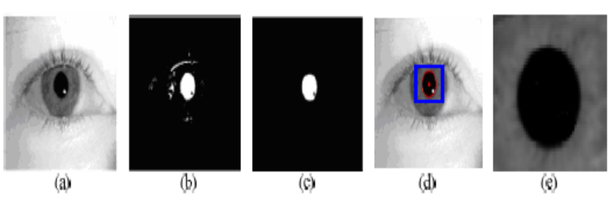

Fig. 2 (a) Eye image (b) Connected components (c) Component with maximum area (d) Pupil and iris detection (e) Segmented image

A normalised bounding box is defined to extract the segmented image based on the pupil detection as shown in Figure 2(d). The segmented image shown in Figure 2(e) consists iris portion surrounding the pupil. The texture in this part of image show maximum randomness to form unique patterns.

4.2 Wavelet Decomposition

An image *I* of size MxN is considered. The one-dimensional DWT applied to each row produces two MxN/2 images. Further, DWT is applied column-wise on these two images to obtain four M/2xN/2 images. The approximation component, app_{comp} represents the coarser information of the input image. The wavelets measure gray level variations in three orientations. The detail information is contained in the horizontal, vertical and diagonal coefficients denoted as hor_{comp}, ver_{comp} and dia_{comp}. The variations along columns represent the horizontal details, the variations along rows gives the vertical details and the variations in the diagonal direction gives the diagonal coefficients [17]. DWT was applied for the non-core segments, $ncseg_i$ and core segments, $cseg_j$ independently, where $i \in \{1, 2, 3, 4, 5, 8, 9, 11, 12, 13, 14, 15, 16\}$ and $j \in \{6, 7, 10, 11\}$. The core and non-core segments are shown in Figure 3.

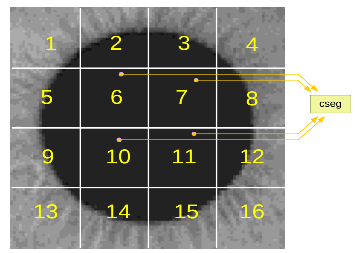

Fig. 3: Segments in iris image

A single level discrete 2-D wavelet transform was applied. The types of wavelet families used are Haar, Daubechies, Symlets, Coiflets and Biorthogonal. The 2D DWT leads to a decomposition of approximation coefficients at level *j* into four components the approximation app_{comp} at level $j+1$, and the details in three orientations, horizontal hor_{comp}, vertical ver_{comp}, and diagonal dia_{comp}. The decomposition is given by (9).

$$(app_{comp}, hor_{comp}, ver_{comp}, dia_{comp}) = wave\_trans(img) \tag{9}$$

where *img* corresponds to *cseg* and *ncseg* of the image.

The hor_{comp}, ver_{comp} and dia_{comp} coefficient values by applying db4 wavelet transform for each segment are tabulated in Table 1. The coefficient values in core segments of all samples are similar. The values are constant due to the texture of the pupil. The intensity values in this region is less or nearing zero. The coefficient values of *cseg* are eliminated. The values obtained from *ncseg* is significant and used for further processing.

Table 1. Detail coefficient values

segment	hor_{comp}	ver_{comp}	dia_{comp}
$ncseg_1$	0.0765	0.1980	-0.0214
$ncseg_2$	0.0958	0.0623	-0.0145
$ncseg_3$	-0.0346	-0.0577	0.0141
$ncseg_4$	0.0327	-0.0870	0.0062
$ncseg_5$	0.0328	0.1924	0.0049
$ncseg_8$	0.0664	0.1454	0.0124
$ncseg_9$	0.0457	0.2724	-0.0031
$ncseg_{12}$	0.0661	0.1548	0.00099

$ncseg_{13}$	0.0231	-0.0764	0.0165
$ncseg_{14}$	0.1506	-0.0594	-0.0076
$ncseg_{15}$	0.1891	-0.0746	-0.0047
$ncseg_{16}$	-0.1164	-0.1989	0.0223
$cseg_{6}$	-5.3291e-015	2.5121e-015	-4.9304e-032
$cseg_{7}$	-5.3291e-015	2.5121e-015	-4.9304e-032
$cseg_{10}$	-5.3291e-015	2.5121e-015	-4.9304e-032
$cseg_{11}$	-5.3291e-015	2.5121e-015	-4.9304e-032

The approximation and the detail coefficients for $ncseg_8$ of genuine and imposter samples are shown in Figures 4(a)-(d).

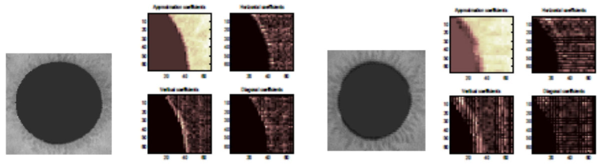

(a) (b) (c) (d)

Fig. 4 (a) Genuine sample (b) db4 wavelet transform applied to $ncseg_8$ of genuine sample (c) imposter sample (d) db4 wavelet transform applied to $ncseg_8$ of imposter sample

It is observed that coefficient values in each segment of genuine and imposter samples are different. The difference is mainly due to the variations in the texture of the iris. The part of the iris close to the pupil show variations between genuine and imposter samples. The wavelet types, Haar, symlets and coiflets are applied on non-segments. The approximation and detail coefficients for $ncseg_8$ are shown in Figures 5(a)-(c).

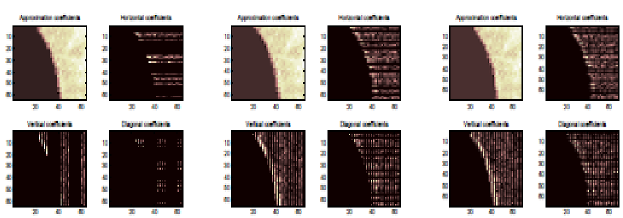

(a) (b) (c)

Fig. 5: (a) Haar wavelet transform (b) Symlets transform (c) Coiflets transform

The coefficient values of *ncseg* are used in summation and magnitude based approaches.

5. SUMMATION BASED APPROACH

The mean values of the horizontal, vertical and diagonal coefficients are denoted by *mhor*, *mver* and *mdia*. The summation of mean values are computed for *ncseg* and *cseg* using (10) and (11).

$$ncs_{hor} = \sum_i mhor(ncseg_i)$$
$$ncs_{ver} = \sum_i mver(ncseg_i) \qquad (10)$$
$$ncs_{dia} = \sum_i mdia(ncseg_i)$$

where i= {1, 2, 3, 4, 5, 8, 9, 12, 13, 14, 15}.

$$cs_{hor} = \sum_j mhor(cseg_j)$$
$$cs_{ver} = \sum_j mver(cseg_j) \qquad (11)$$
$$cs_{dia} = \sum_j mdia(cseg_j)$$

where j= {6, 7, 10, 11}.

The cumulative difference, ratio, z-norm and Pearson correlation coefficient of the summation values along the three orientations are computed. The cumulative difference of the summation values along the three orientations are computed using (12).

$$diff_{ncs} = ns_{dia} - ns_{ver} - ns_{hor}$$
$$diff_{cs} = cs_{dia} - cs_{ver} - cs_{hor} \qquad (12)$$

Ratio of differences is given by $rdiff=diff_{ncs}/diff_{cs}$. The *rdiff* values are in different range for genuine and imposter samples. The *rsum* given by (13) indicates the ratio of the summation values in horizontal and vertical directions of non-core segments with respect to core segments. The values of imposter samples differ from that of the genuine.

$$rsum = (ncs_{hor} + ncs_{ver}) / (cs_{hor} + cs_{ver}) \qquad (13)$$

Table 2: Difference and ratio of summation values for genuine samples

Sample	$diff_{ncs}$	$diff_{cs}$	*rdiff*	*rsum*
1	-8.32E-01	-3.43E-14	2.12E+13	2.58E+13
2	-8.73E-01	-3.83E-14	1.95E+13	2.03E+13
3	-7.94E-01	-3.13E-14	2.05E+13	2.09E+13
4	-8.10E-01	-3.44E-14	2.03E+13	2.04E+13

Table 3: Difference and ratio of summation values for imposter samples

Sample	$diff_{ncs}$	$diff_{cs}$	*rdiff*	*rsum*
1	-2.04E+01	-3.72E-13	6.05E+12	6.42E+12
2	-2.64E+01	-3.24E-13	5.24E+12	5.41E+12
3	-2.11E+01	-2.72E-13	6.47E+12	6.59E+12
4	-2.33E+01	-3.14E-13	5.26E+12	4.36E+12

The summation, $hv_i = ncs_{hor}+ncs_{ver}+cs_{hor}+cs_{ver}$ is calculated where i={1,2,3,4,5,6,7,8,9,10} maps to wt_{order}. The wt_{order} corresponds to the different types of wavelets applied in the order, {db3, db2, db1, db4, db5, db6, Haar, sym, coif, biof}.

The successive differences of the summation values, *dhv* is computed by (14). For instance, the dhv_3 values represent the difference of *hv* values for db1 and db4 transforms. The values prove divergent for genuine and imposter samples.

$$dhv_j = hv_{j+1} - hv_j \text{ where } j=\{1, 2, 3, 4, 5, 6, 7, 8, 9\} \qquad (14)$$

The experiment was continued by estimating successive ratios of the *hv* values. The successive ratios *rhv* values are calculated according to wt_{order}. For instance, the rhv_3 values denotes the ratio of *hv* values by applying db1 and db4 wavelet transform. The *rhv*

values for genuine samples are given in Table 4. The *rhv* values for imposter samples are given in Table 5. The values are different for genuine and
imposter samples.

Table 4. *rhv* values for genuine samples

Sample	rhv_1	rhv_2	rhv_3	rhv_4	rhv_5	rhv_6	rhv_7	rhv_8	rhv_9
1	1.1	0.7	1.2	0.9	1.1	1.1	0.8	0.9	1.2
2	1.1	0.7	1.3	0.7	1.1	2.1	0.5	0.9	1.9
3	0.9	1.5	1.4	0.5	1.1	2.1	0.2	1.3	2.2
4	1.0	1.2	1.3	0.6	1.1	2.4	0.3	0.7	2.4
5	1.7	1.5	1.4	0.2	0.9	2.5	0.2	0.2	2.1
6	1.2	0.9	1.4	0.4	1.2	2.3	0.6	0.5	1.9
7	1.1	0.7	1.3	0.7	1.0	1.4	0.9	0.7	1.4

Table 5. *rhv* values for imposter samples

Sample	rhv_1	rhv_2	rhv_3	rhv_4	rhv_5	rhv_6	rhv_7	rhv_8	rhv_9
1	2.7	3.9	2.5	3.6	4.6	3.4	3.2	4.2	3.7
2	3.0	4.2	2.7	3.2	4.0	4.2	3.6	4.2	4.1
3	2.7	3.6	2.7	3.5	4.6	3.1	4.3	3.8	4.3
4	2.8	4.5	2.6	3.3	4.1	4.3	3.9	4.3	3.8
5	3.1	3.8	2.6	3.2	4.1	3.9	4.3	3.7	4.3
6	3.1	3.7	2.5	2.8	3.8	3.4	3.7	3.7	4.4
7	3.2	3.1	2.6	3.5	4.5	3.4	4.5	3.8	4.3

The z-score was applied for providing promising results. The z-score, Z_i was computed for *hv* values with *i*={1..10}, indicating the type of the wavelet in wt_{order}. The z-score indicates the deviation of *hv* values with respect to the mean and in terms of the standard deviation. The z-score is computed as $Z_i = (x - \overline{x}) / \sigma$ where Z is the z-score, *x* is the *hv* values, $\overline{x}$ is the mean of the *hv* values and σ is the standard deviation. The plot of Z_4 values for genuine and imposter samples is given in Figure 6. It was observed that z-score values of genuine vary from that of an imposter. Z_4 corresponds to db4 wavelet type.

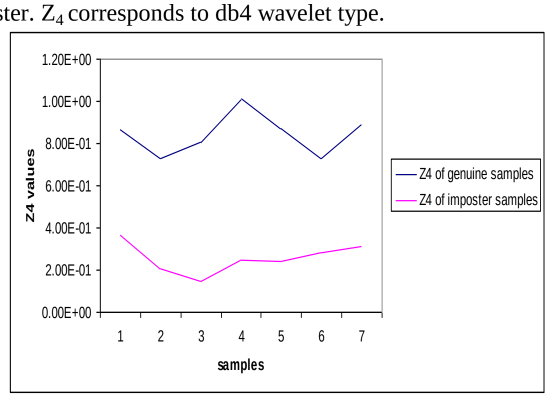

Fig. 6 Plot of z-score of of *hv* values

The Pearson correlation coefficient was computed. The correlation gives the measure of the linear dependence between two values. The correlation was computed for each consecutive *hv* values. The correlation ρ for the values *x* and *y* is calculated using $\rho_j = \text{cov}(x, y) / \sigma_x \sigma_y$ where $x = hv_j$, $y = hv_{j+1}$ such that *j={1,...,9}*. The *x* and *y* are the *hv* values of different wavelets in wt_{order} and σ_x, σ_y denotes its standard deviation. The *cov(x, y)* indicates the covariance of x and y values such that $\text{cov}(x, y) = \sum_{i=1}^{n} (x_i - \overline{x})(y_i - \overline{y})$ where $\overline{x}$ and $\overline{y}$ are the mean values. The correlation values for genuine and imposter samples are given in Table 6.

Table 6. Correlation coefficient values

Sample	ρ_1	ρ_2	ρ_3	ρ_4	ρ_5	ρ_6	ρ_7	ρ_8	ρ_9
genuine	0.9	0.8	0.7	0.8	0.9	0.8	0.9	0.9	0.8
imposter	0.3	0.2	0.3	0.1	0.2	0.1	0.2	0.2	0.1

6. MAGNITUDE BASED APPROACH

The magnitude of horizontal, vertical and diagonal coefficients are denoted as hm_i, vm_i and dm_i where *i*= {1, 2, 3, 4, 5, 8, 9, 12, 13, 14, 15}. The magnitude values follow a particular sequence of transition. Observing *hm*, *vm* and *dm* values of any *ncseg*, the two transition types are learnt. In the first type, the change in magnitude values is from lower to higher and again to lower with reference to *hm*, *vm* and *dm* values respectively. The kind of transition is denoted by P. In the second type, the transition is from higher values in *hm* to lower values in the *vm* and *dm*. The kind of transition is denoted by R. Figure 7 show the transitions.

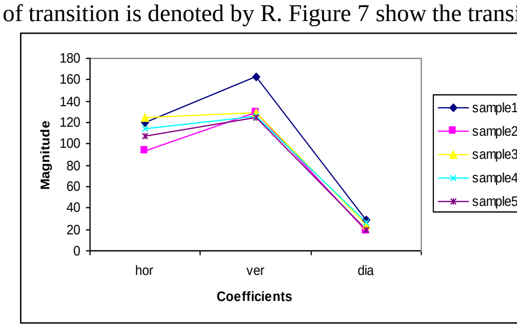

(a)

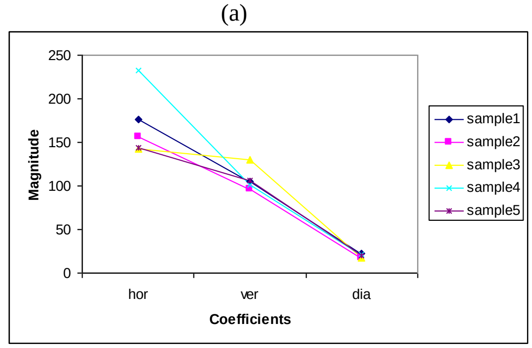

(b)

Fig. 7: (a) P transition (b) R transition

hm_1	120.4219	93.591	124.4134	114.6235	106.8058	
vm_1	163.0247	129.1682	119.3291	105.4855	124.207	P
dm_1	29.0678	18.3647	24.3148	26.348	19.4928	
hm_2	176.2551	155.7625	143.0559	232.4835	143.9673	
vm_2	105.5376	96.0573	130.4328	100.6702	106.0897	R
dm_2	22.2511	17.5944	17.0776	21.7203	20.2583	
hm_3	202.9921	140.729	151.508	171.3156	150.0667	
vm_3	107.3262	103.0724	88.4185	77.1507	101.0765	R
dm_3	25.8415	19.525	18.4014	27.6688	17.7802	
hm_4	109.0968	108.3923	106.3876	135.1441	164.0136	
vm_4	123.1146	123.0885	114.1143	110.8137	126.4034	P
dm_4	22.9881	21.4056	28.5612	29.6903	18.7783	
hm_5	77.6371	83.7933	96.2853	181.0594	85.7155	
vm_5	157.8558	161.1474	169.7154	154.6942	167.8911	P
dm_5	18.8904	16.408	23.7983	32.2722	17.7592	
hm_8	80.7927	97.5364	70.5964	172.8682	121.741	
vm_8	240.6931	168.3456	233.5032	166.8765	183.1311	P
dm_8	28.8119	28.4461	18.9761	35.7735	25.1738	
hm_9	78.6102	99.3977	117.7452	128.9006	168.7103	
vm_9	148.6564	181.4676	195.1323	177.4706	163.9607	P
dm_9	19.7556	21.6574	22.4826	25.1472	27.0723	
hm_{12}	76.5494	90.4139	70.1664	219.2964	111.212	
vm_{12}	243.7948	206.6186	257.3695	207.8282	203.1521	P
dm_{12}	22.0159	26.0787	19.5194	43.9282	26.3994	
hm_{13}	114.7435	122.0762	111.5923	123.5527	184.4414	
vm_{13}	146.2331	132.349	138.6707	114.4425	127.1855	P
dm_{13}	28.6009	22.4014	23.9707	25.3584	27.6726	
hm_{14}	226.6889	166.9654	234.0201	275.4573	178.8402	
vm_{14}	123.1375	122.3672	115.75	103.7045	103.6126	R
dm_{14}	26.2534	20.2562	25.0449	26.0648	18.7733	
hm_{15}	230.2551	177.7625	216.9691	316.1408	172.6033	
vm_{15}	94.5632	118.1518	96.6758	80.2872	126.5293	R
dm_{15}	22.4881	19.6143	20.7141	26.6649	20.7859	
hm_{16}	125.6274	113.4736	133.1699	168.283	138.6666	
vm_{16}	163.0281	159.9156	167.2812	140.0951	141.7218	P
dm_{16}	26.928	25.7717	25.7481	33.7137	28.7091	

Fig. 8: Formation of a *pattern*

The sequence of P and R follow a particular pattern for a subject. For instance, a *pattern*={ P, R, R, P, P, P, P, P, P, P, P, P }. The sequence is in the order considering $ncseg_i$ where i={1, 2, 3, 4, 5, 8, 9, 12, 13, 14, 15, 16}. The formation of a pattern is shown in Figure 8.

hm_1	120.4219	93.591	124.4134	114.6235	106.8058	
vm_1	163.0247	129.1682	119.3291	105.4855	124.207	P
dm_1	29.0678	18.3647	24.3148	26.348	19.4928	
hm_2	176.2551	155.7625	143.0559	232.4835	143.9673	
vm_2	105.5376	96.0573	130.4328	100.6702	106.0897	R
dm_2	22.2511	17.5944	17.0776	21.7203	20.2583	
hm_3	202.9921	140.729	151.508	171.3156	150.0667	
vm_3	107.3262	103.0724	88.4185	77.1507	101.0765	R
dm_3	25.8415	19.525	18.4014	27.6688	17.7802	
hm_4	109.0968	108.3923	106.3876	135.1441	164.0136	
vm_4	123.1146	123.0885	114.1143	110.8137	126.4034	P
dm_4	22.9881	21.4056	28.5612	29.6903	18.7783	
hm_{13}	114.7435	122.0762	111.5923	123.5527	184.4414	
vm_{13}	146.2331	132.349	138.6707	114.4425	127.1855	P
dm_{13}	28.6009	22.4014	23.9707	25.3584	27.6726	
hm_{14}	226.6889	166.9654	234.0201	275.4573	178.8402	
vm_{14}	123.1375	122.3672	115.75	103.7045	103.6126	R
dm_{14}	26.2534	20.2562	25.0449	26.0648	18.7733	
hm_{15}	230.2551	177.7625	216.9691	316.1408	172.6033	
vm_{15}	94.5632	118.1518	96.6758	80.2872	126.5293	R
dm_{15}	22.4881	19.6143	20.7141	26.6649	20.7859	
hm_{16}	125.6274	113.4736	133.1699	168.283	138.6666	
vm_{16}	163.0281	159.9156	167.2812	140.0951	141.7218	P
dm_{16}	26.928	25.7717	25.7481	33.7137	28.7091	

Fig. 9: Formation of a pattern after elimination of segments {5,6,8,9}

Table 7. Pattern types for subjects in ICE database

Pattern No.	Pattern	Subjects
1	P R R P P R R P	3, 6, 17, 24, 27, 28, 51
2	P R R R P R R P	1, 13, 16, 21, 43, 44
3	P R R R P R R R	9, 50, 57, 26, 45, 87
4	P P R R P R R P	14, 7, 47, 10, 19, 78, 80
5	P R R R R R R R	15, 22
6	R R R R P R R P	18, 34, 53, 75, 56, 76, 86
7	R R R R R P P P	32, 79, 81, 83
8	P P P P R R R P	33, 54, 38
9	P P P P P R R P	35, 62, 4, 5, 23, 39, 41
10	P R R P R R R P	63, 49, 66
11	P R R P P R R R	68, 12, 58, 72, 23
12	R R R P P R R P	74, 88
13	P R P P P R R P	8, 65
14	P P P P R R R P	11, 42, 67
15	P R R R R R R P	30, 95
16	P P R P P R R P	46, 59, 89
17	P R P P P R R P	60, 70, 82, 106
18	P R R P R R R R	77, 61, 2
19	R R R P R R R P	85, 29, 37, 48
20	P R R P P P P P	52, 55, 64, 69, 71
21	R R R P P P P P	25, 31, 40
22	R P R P R R R R	20, 36, 84

In segments, $ncseg_5$, $ncseg_8$, $ncseg_9$ *and* $ncseg_{12}$, the transitions are only of type P in all samples. The variations in the segments are negligible. Eliminating the segments in the sequence, the generation of a pattern is shown in Figure 9. The listing of patterns and subjects are given in Table 7.

The *hm*, *vm* and *dm* values are segregated as shown in Figure 10. The minimum average and maximum average values are computed using the averages of each row. The minimum average segments, $minavg_{seg}$ and maximum average segments, $maxavg_{seg}$ are determined for each of the *hm*, *vm* and *dm* values. For instance, $minavg_{seg}=\{hm_1, vm_3, dm_2\}$ and $maxavg_{seg}=\{hm_{15}, vm_{16}, dm_{16}\}$ as shown in Figure 11.

hm_1	120.4219	93.591	124.4134	114.6235	106.8058
hm_2	176.2551	155.7625	143.0559	232.4835	143.9673
hm_3	202.9921	140.729	151.508	171.3156	150.0667
hm_4	109.0968	108.3923	106.3876	135.1441	164.0136
hm_{13}	114.7435	122.0762	111.5923	123.5527	184.4414
hm_{14}	226.6889	166.9654	234.0201	275.4573	178.8402
hm_{15}	230.2551	177.7625	216.9691	316.1408	172.6033
hm_{16}	125.6274	113.4736	133.1699	168.283	138.6666

vm_1	163.0247	129.1682	119.3291	105.4855	124.207
vm_2	105.5376	96.0573	130.4328	100.6702	106.0897
vm_3	107.3262	103.0724	88.4185	77.1507	101.0765
vm_4	123.1146	123.0885	114.1143	110.8137	126.4034
vm_{13}	146.2331	132.349	138.6707	114.4425	127.1855
vm_{14}	123.1375	122.3672	115.75	103.7045	103.6126
vm_{15}	94.5632	118.1518	96.6758	80.2872	126.5293
vm_{16}	163.0281	159.9156	167.2812	140.0951	141.7218

dm_1	29.0678	18.3647	24.3148	26.348	19.4928
dm_2	22.2511	17.5944	17.0776	21.7203	20.2583
dm_3	25.8415	19.525	18.4014	27.6688	17.7802
dm_4	22.9881	21.4056	28.5612	29.6903	18.7783
dm_{13}	28.6009	22.4014	23.9707	25.3584	27.6726
dm_{14}	26.2534	20.2562	25.0449	26.0648	18.7733
dm_{15}	22.4881	19.6143	20.7141	26.6649	20.7859
dm_{16}	26.928	25.7717	25.7481	33.7137	28.7091

Fig. 10: Separation of *hm*, *vm* and *dm* values for a *pattern*

hm_1	120.4219	93.591	124.4134	114.6235	106.8058	→ Minimum average row
hm_2	176.2551	155.7625	143.0559	232.4835	143.9673	
hm_3	202.9921	140.729	151.508	171.3156	150.0667	
hm_4	109.0968	108.3923	106.3876	135.1441	114.0136	
hm_{13}	114.7435	122.0762	111.5923	103.5527	124.4414	
hm_{14}	226.6889	166.9654	234.0201	275.4573	178.8402	
hm_{15}	230.2551	177.7625	216.9691	316.1408	172.6033	→ Maximum average row
hm_{16}	125.6274	113.4736	133.1699	128.283	138.6666	

vm_1	163.0247	129.1682	129.3291	125.4855	124.207	
vm_2	105.5376	96.0573	130.4328	100.6702	106.0897	
vm_3	107.3262	103.0724	88.4185	77.1507	101.0765	→ Minimum average row
vm_4	123.1146	123.0885	114.1143	140.8137	126.4034	
vm_{13}	146.2331	132.349	138.6707	114.4425	127.1855	
vm_{14}	123.1375	122.3672	115.75	103.7045	103.6126	
vm_{15}	94.5632	118.1518	96.6758	80.2872	126.5293	
vm_{16}	163.0281	159.9156	167.2812	140.0951	141.7218	→ Maximum average row

dm_1	29.0678	18.3647	24.3148	26.348	19.4928	
dm_2	22.2511	17.5944	17.0776	21.7203	20.2583	→ Minimum average row
dm_3	25.8415	19.525	18.4014	27.6688	17.7802	
dm_4	22.9881	21.4056	28.5612	29.6903	18.7783	
dm_{13}	28.6009	22.4014	23.9707	25.3584	27.6726	
dm_{14}	26.2534	20.2562	25.0449	26.0648	18.7733	
dm_{15}	22.4881	19.6143	20.7141	26.6649	20.7859	
dm_{16}	26.928	25.7717	25.7481	33.7137	28.7091	→ Maximum average row

Fig. 11 Minimum and maximum average values for a pattern

7. EXPERIMENTAL RESULTS

Experiments are conducted on ICE database [18]. The database consists of 89 subjects with 7 samples per subject. The wavelet based recognition use magnitude values of the coefficients. A unique code is generated for each subject. The code recognizes a person from others in the database. $minavg_{seg}$ and $maxavg_{seg}$ values represent the code for an individual. The recognition rate is 100%. Table 8 depicts $minavg_{seg}$ and $maxavg_{seg}$ values for first and second level of decomposition. The sequence indicates *hm*, *vm* and *dm* values of $minavg_{seg}$ and $maxavg_{seg}$. For instance, level 1 entry for subject 1 is {*hm*1, *vm*2, *dm*3, *hm*15, *vm*16, *dm*16}. The first three values {*hm*1, *vm*2, *dm*3} correspond to $minavg_{seg}$. The next three values {*hm*15, *vm*16, *dm*16} correspond to $maxavg_{seg}$ values. The values are unique for each person in the database.

Table 8. $minavg_{seg}$ and $maxavg_{seg}$ values for first and second level wavelet decomposition for ICE database

Subject	Level 1 decomposition	Level 2 decomposition
1	hm_1, vm_2, dm_3, hm_{15}, vm_{16}, dm_{16}	hm_{13}, vm_1, dm_3, hm_3, vm_2, dm_1
2	hm_4, vm_{15}, dm_3, hm_{15}, vm_1, dm_1	hm_3, vm_{15}, dm_4, hm_{15}, vm_2, dm_1
3	hm_1, vm_{14}, dm_{16}, hm_{15}, vm_1, dm_{13}	hm_1, vm_{15}, dm_3, hm_{14}, vm_1, dm_{13}
4	hm_2, vm_4, dm_{13}, hm_1, vm_{16}, dm_{13}	hm_4, vm_4, dm_2, hm_{13}, vm_{16}, dm_{13}
. . .	. . .	. . .
88	hm_4, vm_{15}, dm_3, hm_1, vm_{13}, dm_{13}	hm_1, vm_2, dm_3, hm_4, vm_{13}, dm_{15}
89	hm_2, vm_4, dm_{13}, hm_{14}, vm_4, dm_2	hm_{14}, vm_{15}, dm_2, hm_1, vm_3, dm_4

8. CONCLUSION

Wavelet transformation is applied for the non-core components. The non-core components are the regions which show variations in the texture and intensity values. The summation and magnitude values of the detailed coefficients form a specific representation for recognition. The summation based method implements different type of wavelets, Haar, db4, symlets, coiflets and biorthogonal. The results obtained using db4 are promising for recognition. The magnitude of detail coefficients is the basis for generation of unique code. The identification of unique code for each person is the novel recognition process.

9. ACKNOWLEGMENTS

The authors would like to thank Patrick J Flynn, Professor, Department of Computer Science and Engineering, University of Notre Dame, USA for providing ICE database.

10. REFERENCES

[1] Rafeal C. Gonzalez and Richard E. Woods. 2005. Digital Image Processing, 2nd Edition, Pearson Education.

[2] C.A.Bouman. 2011. Connected Component Analysis, Digital Image Processing, *https://engineering.purdue.edu/bouman/ece637/notes/pdf/ConnectComp.pdf.*

[3] Abeer George Ghuneim. 2000. Defining Connectivity, *http://www.imageprocessingplace.com.*

[4] Earl Gose, Richard Johnsonbaugh and Steve Jost. 2006. Pattern Recognition and Image Analysis, 1st Edition, Prentice-Hall of India Private Limited.

[5] Robi Polikar. 1999. The Wavelet Tutorial.

[6] Amara Graps. 1995. An Introduction to Wavelets, Computing in Science and Engineering, vol. 2, no. 2, pp. 50-61.

[7] Mohammed A. Salem, Nivin Ghamry and Beate Meffert. 2009. Daubechies Versus Biorthogonal Wavelets for Moving Object Detection in Traffic Monitoring Systems,

http://www2.informatik.hu-berlin.de/sam/preprint/m.

[8] Junxing Ma, Jijun Xue, Shengjun Yang and Zhengjia He. 2003. A study of the construction and application of a Daubechies wavelet-based beam element, Finite Elements in Analysis and Design, vol. 39, pp. 965-975.

[9] J. Daugman. 1993. High Confidence Visual Recognition by a Test of Statistical Independence, IEEE Trans. Pattern Analysis and Machine Intelligence, vol. 15, No.11, pp.1148-1161.

[10] Karen Hollingsworth, Sarah Baker, Sarah Ring, Kevin W. Bowyer and Patrick J.Flynn. 2009. Recent Research Results In Iris Biometrics, SPIE 7306B: Biometric Technology for Human Identification VI.

[11] R. Wildes, J. Asmuth, G. Green, S. Hsu, R. Kolczynski, J. Matey, and S. McBride. 1996. A machine-vision system for iris recognition, Mach. Vis. Applic., vol. 9, pp. 1-8.

[12] Li Ma, Tieniu Tan, Yunhong Wang, Dexin Zhang. 2003. Personal Identification based on Iris Texture Analysis, IEEE Transactions on Pattern Analysis and Machine Intelligence, Vol.25, No.12, pp. 1519-1533.

[13] Zhenan Sun, Yunhong Wang, Tieniu Tan and Jiali Cui, 2004. Improving Iris Recognition Accuracy Via Cascaded Classifiers, Biometric Authentication. LNCS 3072, pp. 1-11.

[14] H. Proena and L.A. Alexandre. 2006. Iris Segmentation Methodology for Noncooperative Iris Recognition. IEE Proc. Vision, Image, and Signal Processing, vol. 153, no. 2, pp. 199-205.

[15] Aditya Abhyankar and Stephanie Schuckers. 2010. Novel Biorthogonal Wavelet based Iris Recognition for Robust Biometric System, International Journal of Computer Theory and Engineering, vol. 2, No. 2, pp. 1793-8201.

[16]Agus Harjoko, Sri Hartati and Henry Dwiyasa. 2009. A Method for Iris Recognition Based on 1D Coiflet Wavelet.World Academy of Science, Engineering and Technology, vol. 56, pp. 1-4.

[17] Zhengmao Ye, Yongmao Ye, Hang Yin, Habib Mohamadian. 2009. Integration of Wavelet Fusion and Adaptive Contrast Stretching for Object Recognition with Quantitative Information Assessment, ICGST-GVIP Journal, vol. 8, Issue V, pp. 33-42.

[18]Xiaomei Liu, Bowyer K.W. and Flynn P.J. 2005. Experimental Evaluation of Iris Recognition, IEEE Computer Society Conference on Computer Vision and Pattern Recognition Workshops, pp. 158-165.